REPORT DOCUMENTATION PAGE

Public Reporting burden for this collection of information is estimated to average 1 hour per response, including the time for reviewing instructions, searching existing data sources, gathering and maintaining the data needed, and completing and reviewing the collection of information. Send comment regarding this burden estimates or any other aspect of this collection of information. including suggestions for reducing this burden, to Washington Headquarters Services, Directorate for information Operations and Reports, 1215 Jefferson Davis Highway, Suite 1204, Arlington, VA 22202-4302, and to the Office of Management and Budget, Paperwork Reduction Project (0704-0188,) Washington. DC 20503.

1. AGENCY USE ONLY (Leave Blank)	2. REPORT DATE 10 October 2001	3. REPORT TYPE AND DATES COVERED Final 15Jul96 - 14Jul01

4. TITLE AND SUBTITLE Free-Piston Linear Alternator for Auxiliary Power Unit	5. FUNDING NUMBERS Grant #DAAH04-96-1-0328

6. AUTHOR(S)
Drs. P. Famouri, N, Clark, C. Atkinson

7. PERFORMING ORGANIZATION NAME(S) AND ADDRESS(ES) West Virginia University College of Engineering and Mineral Resources Evansdale Drive, 747 Engineering Sci Bldg Morgantown, WV 26506-6109	8. PERFORMING ORGANIZATION REPORT NUMBER EMS-10-01

9. SPONSORING / MONITORING AGENCY NAME(S) AND ADDRESS(ES) U. S. Army Research Office P.O. Box 12211 Research Triangle Park, NC 27709-2211	10. SPONSORING / MONITORING AGENCY REPORT NUMBER 36200.3-RT-DPS

11. SUPPLEMENTARY NOTES
The views, opinions and/or findings contained in this report are those of the author(s) and should not be construed as an official Department of the Army position, policy or decision, unless so designated by other documentation.

12 a. DISTRIBUTION / AVAILABILITY STATEMENT Approved for public release; distribution unlimited.	12 b. DISTRIBUTION CODE

13. ABSTRACT (Maximum 200 words)

14. SUBJECT TERMS	15. NUMBER OF PAGES 61
	16. PRICE CODE

17. SECURITY CLASSIFICATION OR REPORT UNCLASSIFIED	18. SECURITY CLASSIFICATION ON THIS PAGE UNCLASSIFIED	19. SECURITY CLASSIFICATION OF ABSTRACT UNCLASSIFIED	20. LIMITATION OF ABSTRACT UL

RECEIVED
OCT 1 8 2001
By
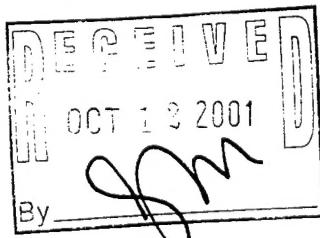
20011023 044

Final Report

On

Free-Piston Diesel-Fueled Linear Alternator for

Auxiliary Power Unit Applications

Grant no. *DAAH04-96-1-0238*

From 1996 thorough 1999

prepared by

Departments of

Electrical and Computer Engineering

and

Mechanical and Aerospace Engineering

West Virginia University

Principal Investigators: Christopher Atkinson, Parviz Famouri, Nigel Clark

Author: Samuel Taylor

Prepared for

U.S. Army Research Office

and

Defense Advanced Research Project Agency

Table of Contents

Spark Ignited Linear Engine Development

Introduction

Present day internal combustion engines have been proven to be a successful means of converting linear reciprocating motion into rotary motion through the use of a slider-crank mechanism. However, a substantial portion of the mechanical work produced is lost in internal friction due to the presence of moving parts, like the crankshaft. The use of a linear engine to eliminate the crankshaft and other rotating components would eliminate these sources of friction, and hence improve the overall efficiency of the engine. Further advantages of this engine configuration are those of reduced weight and cost, from the reduction of components required. Previous studies of free-piston engine designs have indicated that they would be useful where linear power delivery could be used, such as in fluid power delivery, or in electrical energy applications.

The first prototype engine design considered consisted of two pistons, connected solidly by a rod, such that the two pistons reciprocated with precisely the same motion. The motion of the piston was not mechanically prescribed, but was rather the result of the balance of in-cylinder pressures, inertial forces, frictional forces, and the applied load. Idealized modeling of a two-stroke linear engine, assuming Otto cycle operation, yielded a closed form solution for piston motion, but compression ratio provided the only degree of freedom to allow variable efficiency. A benchtop model of this configuration was constructed and tested. The initial prototype was a gasoline fueled spark-ignited engine, and was successfully tested under various operating conditions. In-cylinder pressure data and piston position data were recorded. The idealized mathematical model was utilized

to conduct analysis into the effects of varying air-fuel ratios, compression ratios, and engine sizes on the engine operating speed, an important parameter in the conversion of chemical energy input to the engine to electrical energy output from the alternator.

Free Piston Engine Modeling and Analysis

A fundamental analysis was undertaken by Nandkumar (1998) in order to provide a basic understanding of the linear two-cylinder internal combustion engine, much in the way an air standard Otto cycle or Diesel cycle provides basic understanding of engine thermodynamic trends. The idealized model used in the analysis consisted of a linear two-cylinder two-stroke cycle internal combustion engine that follows an idealized Otto cycle of operation. The assumptions used in carrying out this modeling were:

1. A two stroke engine concept was assumed which follows an idealized Otto cycle for its operation, i.e. instantaneous intake and exhaust at the innermost position and instantaneous heat release at the outermost position

2. An idling case of operation with only a frictional force being encountered during the engine operation was used to simplify the modeling.

3. The heat input to the engine was used entirely for the work done to overcome the friction drag force acting on the piston (no heat loss)

The analysis was carried out in dimensionless form. Given these assumptions, an analytical solution in velocity versus position, velocity versus time, and position versus time were obtained.

Mathematical Model

When considering a linear two-stroke engine model the following variables may be specified,

b   bore

x_m maximum theoretical half-stroke length

F_f friction force required to move the slider

m_s mass of the slider

Q_{in} quantity of heat added

P_m midpoint pressure of the cylinder compression

n   ratio of specific heats (assumed to be known)

With these variables the force balance for a left-to-right stroke with x positive in the left-to-right direction is:

$$P_1(x)\frac{\pi b^2}{4} - P_2(x)\frac{\pi b^2}{4} - F_f - m_s\frac{d^2x}{dt^2} = 0 \quad (1\text{-}1)$$

After further analysis it can be found that

$$\frac{\pi b^2}{4}P_u\left[\frac{x_m^n}{(x_m-x)^n}\right] - \frac{\pi b^2}{4}P_m(x)\left[\frac{x_m^n}{(x_m-x)^n}\right] - F_f - m\frac{d^2x}{dt^2} = 0 \quad (1\text{-}2)$$

with P_u the unknown midpoint pressure for the left side.

The relationship between P_u and P_m depends on the heat added, Q_{in}, and the steady state stroke of the engine.

The minimum volume for such an engine is

$$\frac{\pi b^2}{4}(x_m - x_s)$$

and maximum is

$$\frac{\pi b^2}{4}(x_m + x_s).$$

Hence the compression ratio, r, is given by

$$r = \frac{x_m + x_s}{x_m - x_s} \quad (1\text{-}3)$$

The mechanical work done in one stroke is

$$W_f = 2F_f x_s$$

After invoking Otto cycle efficiency, it can be concluded that

$$2F_f x_s = Q_{in}\left[1 - \left(\frac{x_m - x_s}{x_m + x_s}\right)^{n-1}\right] \quad (1\text{-}4)$$

Also, following an Otto cycle, assuming adiabatic compression and constant volume heat addition, one finds that

$$\frac{P_u}{P_m} = \left[\frac{T_m\left(\dfrac{x_m}{x_m - x_s}\right)^{n-1} + \dfrac{Q_{in}}{m_f C_v}}{T_m\left(\dfrac{x_m}{x_m - x_s}\right)^{n-1}}\right] \quad (1\text{-}5)$$

Equations (2) and (5) may be solved mutually for a given input with the boundary conditions

$$x = -x_s; \quad \frac{dx_s}{dt} = 0$$

$$x = +x_v; \quad \frac{dx_s}{dt} = 0$$

provided that x_s is known. However x_s depends on Q_{in} and is best found using equation (4), which may be given in dimensionless form.

$$\frac{2F_f x_s}{Q_{in}} = \left(\frac{x_m}{x_s}\right)\left[1 - \left(\frac{1 - \dfrac{x_s}{x_m}}{1 + \dfrac{x_s}{x_m}}\right)^{n-1}\right] \quad (1\text{-}6)$$

It should be noted that for a fixed frictional force and maximum theoretical half-stroke length, the ideal fuel quantity Q_{in} is tightly restricted within the constraint of commonly accepted compression ratios. Generally, Q_{in} decreases slowly with increasing stroke for this ideal model. Equation (5) may be re-written as

$$\frac{P_u}{P_m} = \left[1 + \left\{ \frac{Q_{in} \left(\dfrac{x_m}{x_m - x_s} \right)^{1-n} (n-1)}{P_m x_m \left(\dfrac{\pi b^2}{4} \right)} \right\} \right] \quad (1\text{-}7)$$

So that the solution in dimensionless terms is

$$\frac{P_u}{P_m} \left(\frac{1}{\left(1 + \dfrac{x}{x_m}\right)^n} \right) - \left(\frac{1}{\left(1 - \dfrac{x}{x_m}\right)^n} \right) - \frac{F_f x_m}{Q_{in}} \frac{Q_{in}}{P_m x_m \left(\dfrac{\pi b^2}{4} \right)} - \frac{1}{2} \frac{d^2 \left(\dfrac{x}{x_m} \right)}{dt^{*2}} = 0 \quad (1\text{-}8)$$

Where
$$t^* = \frac{t_c}{\sqrt{\dfrac{2m_s x_m}{P_m \left(\dfrac{\pi b^2}{4} \right)}}} \quad (1\text{-}9)$$

Equation (8) proves non-solvable in seeking a solution for position versus time, however, it is possible to obtain an analytic solution for velocity versus position.

Setting $x^* = \dfrac{x}{x_m}$ and setting dimensionless velocity $v^* = \dfrac{dx^*}{dt^*}$

Then equation (8) may be represented as

$$\frac{1}{2} v^* \frac{dv^*}{dx^*} - \left(\frac{P_u}{P_m} \right) \left(\frac{1}{(1 + x^*)^n} \right) + \left(\frac{1}{(1 - x^*)^n} \right) - \frac{F_f x_m}{Q_{in}} \frac{Q_{in}}{P_m x_m \left(\dfrac{\pi b^2}{4} \right)} = 0 \quad (1\text{-}10)$$

Initial Modeling

Based on this mathematical model, analyses were conducted to determine factors affecting the engine frequency of operation, assuming that the pressure in the left and right cylinders varies in the same way with respect to dimensionless time. Two cases, the effect of engine bore on engine speed, and the effect of air-fuel ratio on engine speed. Time is rendered dimensionless in this case with respect to the time period needed to complete a stroke, τ. A simple force balance shows that

$$\tau = \sqrt{\frac{8m_s x_m}{\pi b^2 k}} \quad (1\text{-}11)$$

where k is a constant depending on the exact time-varying in-cylinder pressures. This equation shows us that piston speed will decrease as the square root of the reciprocating mass, but increase as the bore increases. The analysis was conducted for 3 different values of compression ratio, 10, 15, and 20. The bore was varied from 25.4mm (1 in.) to 152.4mm (6 in.). The reciprocating mass was assumed to be 5kg (11lb). The engine was assumed to reciprocate freely with no heat being added and no frictional load being encountered. The numerical value of dimensionless time was converted into dimensional terms using the following equation:

$$t = t^* \times \sqrt{\frac{2m_s x_m}{P_m \left(\frac{\pi b^2}{4}\right)}} \quad (1\text{-}12)$$

where t is in seconds. The results of the analysis are shown below, and engine speed was found to increase with an increase in bore and an increase in compression ratio.

Table 1-1.

The effect of changing the engine bore for different compression ratios

Bore mm (in.)	r = 10 Speed (cpm)	r = 15 Speed (cpm)	r = 20 Speed (cpm)
25.4 (1)	751	915	965
50.8 (2)	1499	1825	1938
76.2 (3)	2249	2744	2900
101.6 (4)	2998	3663	3860
127.0 (5)	3748	4582	4837
152.4 (6)	4511	5488	5798

The power being extracted from the engine by the linear alternator is directly proportional to the speed of the engine. The speed of the engine would vary with the heat input to the system, a function of air-fuel ratio, and with the engine size, a function of the stroke to bore ratio. An analysis was conducted on four different cases of stroke-to-bore ratios, with air-fuel ratios varied from 12 to 50. The compression ratio was assumed to be 20. The heat input to the engine was calculated by using the following equations:

Mass of air (kg/cycle) = Displacement volume * Air Density   (1-13)

Mass of fuel (kg/cycle) = Mass of air per cycle / Air-Fuel Ratio   (1-14)

Heat Input (kJ) = Mass of fuel * Calorific Value of fuel   (1-15)

The heat input was then used to calculate the velocity and displacement of the piston.

It was found that the engine speed reduced with an increase in air-fuel ratio. This can be attributed to the fact that this idealized model treats an increase in air-fuel ratio as a decrease in heat input, and thereby a decrease in piston velocity. The analysis also showed an increase in engine speed with a decrease in stroke-to-bore ratio. Since the final electrical output from the linear alternator is directly proportional to the speed of the engine, it is desirable to increase the engine speed.

Table 1-2.

Effect of varying air-fuel ratio for different stroke-to-bore ratios.

AFR	L/b = 3	L/b = 1.4	L/b = 1	L/b = 0.84
	Speed (cpm)	Speed (cpm)	Speed (cpm)	Speed (cpm)
12	827.8	1624.2	3513.1	5420.0
15	730.5	1407.5	3099.6	4783.1
20	675.2	1284.1	2865.1	4420.5
25	638.8	1200.0	2710.5	4182.6
30	604.5	1151.2	2601.3	4013.1
35	531.3	1115.9	2520.2	3925.5
40	476.8	1042.6	2417.9	3785.8
45	395.5	1032.5	2339.6	3645.1
50	355.3	965.0	2235.6	3430.6

Benchtop Model Construction and Design

A benchtop prototype linear engine was constructed and operated in a gasoline-fueled spark-ignited mode. The benchtop model was sized to use 2-stroke chainsaw engine components to reduce development time and cost. The prototype used a two-stroke cycle, to insure sustainable motion without intervention because each stroke is a power stroke. This also allowed a simple port configuration, rather than a complex camless valve control system. Spark-ignited operation was used to allow low-pressure port fuel injection. The fuel injection used a fuel pump to maintain a common rail at a constant pressure of 103kPa (15psig). Adjusting fuel injector pulse width controlled fuel flow rate. The injectors were pulsed every two strokes. Compressed house air was used to improve scavenging. Airflow was controlled to each cylinder by individual manual valves. Generic automotive ignition coils were selected to provide spark, and the original spark plugs for the heads were used. Coolant water was forced through the heads from the house water supply. A simple I-beam frame provided support for each cylinder. A controller was constructed to fire the motoring coils, as well as control the spark timing

and fuel injection pulse-width. A Hall-effect linear position sensor was designed and constructed, and was the only sensor input to the controller. A simple sketch of the engine configuration and a table of utilized components are shown below.
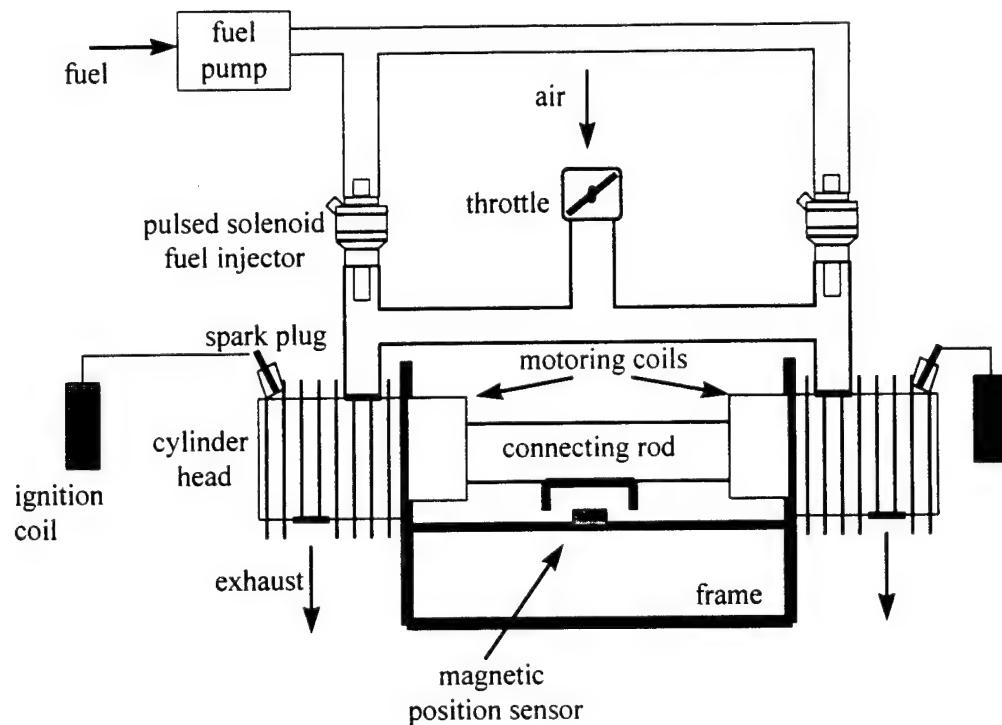

Figure 1-1. Benchtop Model Layout

Table 1-3. Engine Component Description

Component	Description
cylinder heads	Homelite XL2 chainsaw cylinders with integral heads
pistons	33 mm diameter, 1 pinned ring, 45 mm long (fabricated in-house)
connecting rod assembly	main shaft: 30.5 mm diameter round steel bar, 305 mm length piston-to-main shaft: 13 mm diameter, 40 mm long, passing through stepped plug and lip seal
frame	bottom beam: I-beam:100 mm wide, 105 mm high, 600 mm long, web thickness 7.2 mm head supports: angle iron: 102 mm sides, 153 mm long, 18.5 mm thick
throttle	stock item for Homelite XL2
motoring coils	adapted from a generic starter solenoid for a heavy duty automotive engine
fuel injectors	GM Part # 17109448F
fuel pump	Holley Automotive

In order to directly observe the nature of the combustion process in this engine piezoelectric in-cylinder pressure transducers were mounted with direct access to the combustion chamber. The port locations were not optimized, because the stroke of the engine is not mechanically constrained, allowing the optimum port location to vary each cycle. A second variable dependent on the stroke is the compression ratio, which had a theoretical maximum of 8:1 for this engine.

Experimental Results

The 36.5mm bore benchtop model has been operated successfully on gasoline with a lubrication oil mix of 50:1 to preserve and seal the rings. Fuel delivery was electronically metered but controlled manually, and was typically rich to ensure combustion. It was found, as expected, that ignition timing control was crucial to the successful operation of the engine. For example, under no load conditions, there was a tendency for the assembly to hit the stops before motion was reversed, unless timing was advanced so far that adverse work was done in slowing the piston. In the no load

condition it was evident that the only forces slowing the assembly to the point of reversal were the ring and rod friction, and the pressure in the cylinder at its outermost point. This effect of ignition timing would prove less critical with engine of higher compression ratio. The effect of adding load to the engine was accomplished through a crude friction brake. Some plots of output from the linear alternator-engine combination are shown below and Nandkumar's thesis is attached, with further analysis and results.

Linear Alternator Output Power
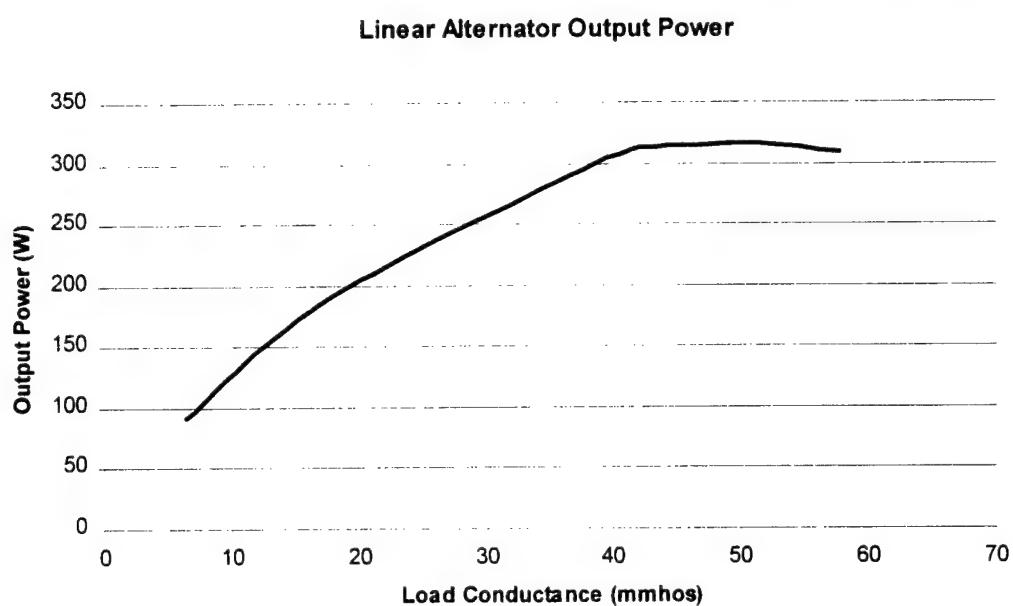
Figure 1-2: Linear Engine-Alternator output power. Peak value 316W. End of run occurred when engine stalled under load.

Actual Alternator Output Voltage Waveform
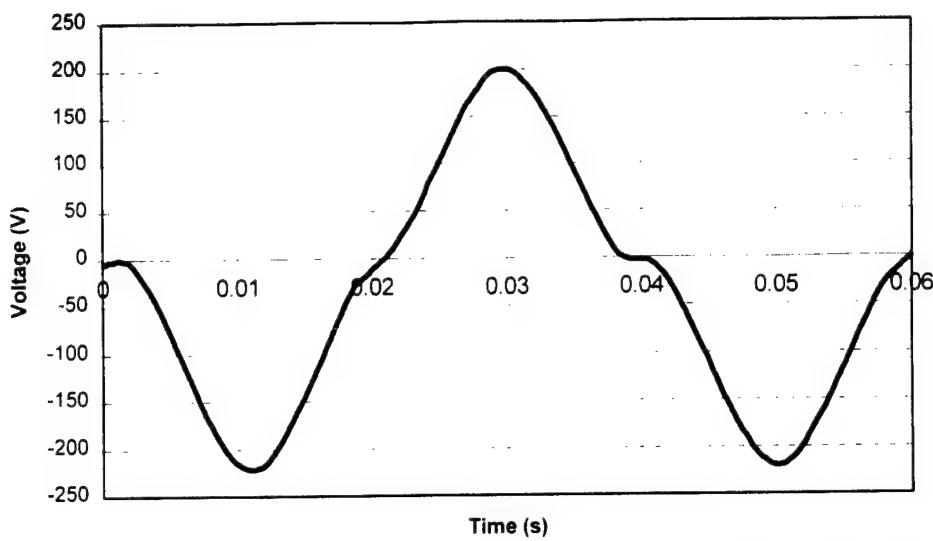
Figure 1-3: Actual linear alternator output voltage. Output voltage waveform of the prototype is nearly sinusoidal.

Table 1-4: Linear Alternator Output Data

TEST	LOAD (ohms)	VOLTAGE (V)	CURRENT (A)	LOAD POWER (W)	FREQUENCY (Hz)
1	OC	132.0	0.00	0	25.0
2	156.0	120.0	0.75	92	24.6
3	130.0	119.0	0.88	104	24.4
4	104.0	115.0	1.07	124	23.4
5	78.0	111.0	1.38	153	24.1
6	52.0	103.0	1.92	200	26.6
7	26.0	90.0	3.30	300	23.6
8	24.0	88.5	3.54	312	23.6
9	23.4	87.5	3.58	313	23.6
10	19.5	79.0	3.90	316	23.1
11	17.3	74.0	4.15	309	22.7
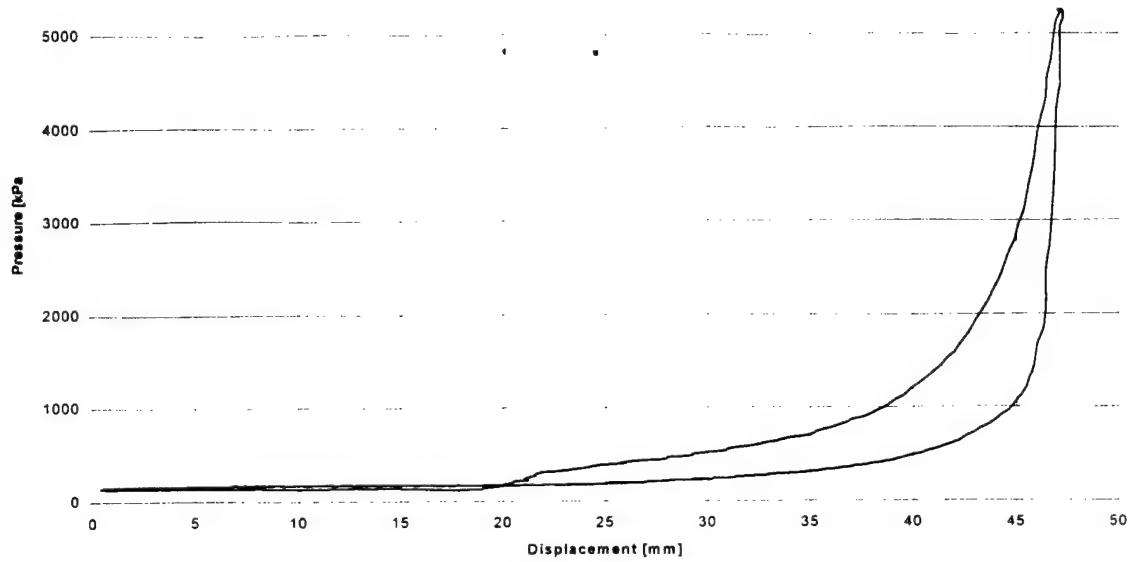
Figure 1-4: Typical Pressure vs. Displacement Diagram, Linear Engine Alternator combination.
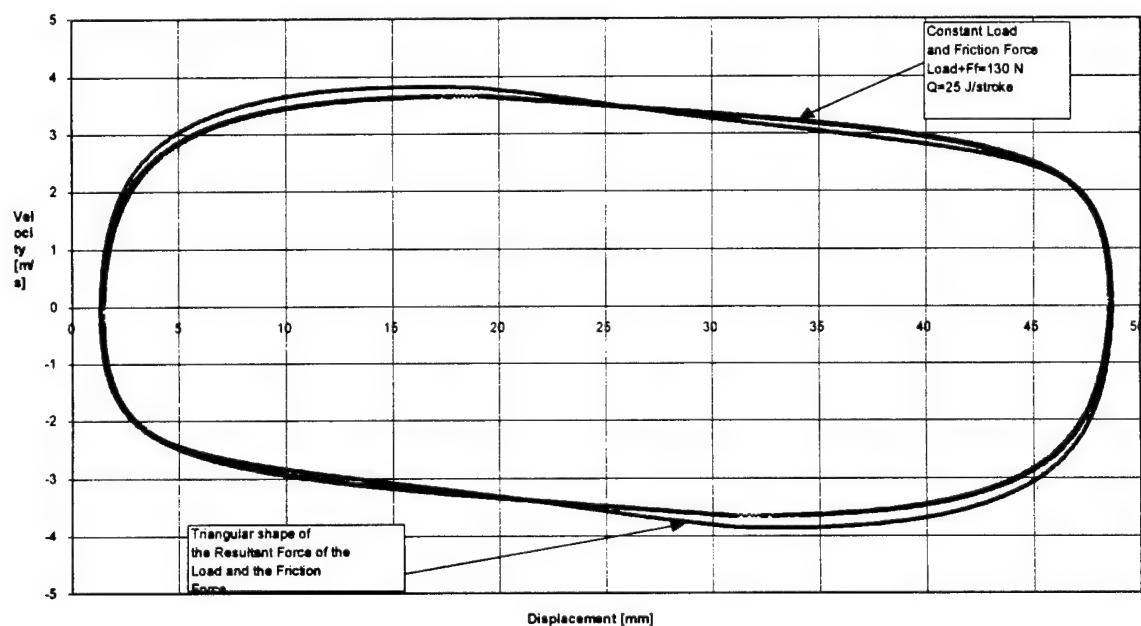
Figure 1-5: Piston Velocity vs. Displacement for different shapes of the Friction Force and Load

Linear Alternator Development

Introduction

The development of the linear alternator presented in this section is focused on the design and construction of a permanent magnet (PM) linear alternator (Cawthorne, 1999). This selection of linear alternator type is not an optimized design choice as different alternator types such as induction and reluctance alternators suitable for this application have yet to be investigated. The PM alternator was selected based on several key advantages of the PM machine including high power density and high strength of the field.

Although the PM alternator does have its advantages, as with any design choice, a trade off does exist between these advantages and the disadvantages associated with PM machines. The major disadvantage of a PM machine is that the field flux of the machine is not controllable. This restriction makes regulating the output voltage of the machine much more difficult. In a synchronous generator, for example, the field flux can be adjusted by varying the current in the field windings. This field flux then determines the output voltage of the machine. Thus, the output voltage of a synchronous generator can easily be regulated by controlling the field current. In a PM machine, the output voltage regulation is not as simple since the field flux is supplied by permanent magnets and is constant. Without the ability to vary the field flux, other methods of regulating the output voltage of the machine such as connecting the machine to a phase controlled rectifier or other power electronic regulation system must be examined.

In addition, the PM configuration does not provide for short circuit protection. In a machine with field control, if a short circuit is detected, the field current to the machine can be turned off which will significantly reduce the machine output voltage and mitigate the damaging the effects of the short circuit. Finally, the PM machine configuration can prove to be expensive due to the high cost of the magnets.

After careful examination of the advantages and disadvantages of the permanent magnet linear alternator concept, the decision was made to pursue this particular machine type. Since two of the objectives of constructing this first prototype machine were to provide proof of the linear engine-alternator concept and to grant insight into the operation of the engine-alternator system as a unit, it was determined that the benefits of the PM machine outweighed the drawbacks. Therefore, the PM configuration was selected for the initial prototype linear alternator.

Linear Alternator Modeling and Analysis

A basic approach for the design of a three-phase tubular linear alternator was intended to be a preliminary design step to provide the basic geometric dimensions of the machine. Information was obtained for determining the diameter of the magnets and of the windings, and also for determining the number of coils necessary to produce the desired voltage magnitudes and the desired power levels. The initial approach did not discuss sizing the magnet thickness, winding thickness, magnet span, and winding span. Rather, it was recommended that the optimum values for these parameters be determined using a finite element analysis package.

For use in the equations developed, the machine speed must be expressed in units of distance per time. If the stroke length is given in inches and the mechanical frequency is given in cycles per minute, the speed, u, can be defined as

$$u = 2\frac{strokes}{cycle} \times f_m \frac{cycles}{min} \times \tau \frac{m}{stroke} \times \frac{1\,min}{60\,sec} = \frac{f_m\tau}{1181}\,m/s \qquad (2\text{-}1)$$

Now, the inner diameter of the machine stator poles necessary to meet the output power requirements of the machine given the mechanical speed and stroke length can be determined using Equation 2-2.

$$D = \frac{S_n}{\pi m_r \sigma_{f_{xr}} u \eta_r} \qquad (2\text{-}2)$$

where

S_n = rated power of the alternator

m_r = number of active rotor poles

τ = pole pitch

f_{xr} = specific thrust

u = machine speed

η = predicted rated efficiency

The number of turns per winding can then be found using Equation 2-3

$$n_s = \frac{\sqrt{2}V_0}{2\omega B_{gr}\tau D m_r} \qquad (2\text{-}3)$$

where

V_0 = rated voltage (RMS)

ω = electrical frequency

B_{gr} = magnet air gap flux density

To examine a number of possible alternator designs, a spreadsheet was developed to calculate the various characteristics based on the desired parameters of the machine. For the existing engine, the stroke length has been determined to be 1.65 inches with a mechanical frequency of 1000 cycles per minute. First, the machine parameters were found by specifying the desired output power and output voltage of the machine. Using the engine parameters specified above, with a desired output power of 500 W and a desired output voltage of 120 V_{RMS} gives the alternator parameters as shown in Table 2-1.

Table 2-1. Alternator Parameters

Output Power	S_n	500	W
Output Voltage	V_0	120	V_{RMS}
Number of Active Rotor Poles	m_r	4	Poles
Pole Pitch	τ	1.65	Inches
Specific Thrust	f_{xr}	1.32	N/cm^2
Machine Speed	U	1.4	m/s
Predicted Rated Efficiency	η	0.80	
Magnet Air Gap Flux Density	B_{gr}	0.65	T
Diameter	D	2.535	Inches
Number of Windings	n_s	289	Turns

Finite Element Analysis and Optimization

Once the basic geometric parameters of the alternator were defined, it was necessary to employ a finite element analysis package to select the remaining parameters (magnet height, magnet span (thickness), winding height, winding span) in such a was so as to optimize the design. Due to its availability and optimization capabilities, the ANSYS package was used to analyze and optimize the design.

First, a parametric model of the entire alternator system was created in the ANSYS environment. In a parametric model, all of the important dimensions are defined with a variable that can be varied to alter the geometry of the model. This allows for easy

manipulation of the model for various design ideas. In addition, the parametric model is used by the ANSYS optimization routines to vary the model as the software optimized the specified parameters of the model to meet predefined performance criteria.

After the parametric model was defined, the ANSYS simulation was setup by defining the materials comprising the alternator, defining the meshing necessary for the finite element analysis, and establishing the boundary conditions. With these steps completed, the analysis for a single machine configuration could be completed. The next step involved implementing the optimization routines. The basic optimization process in the ANSYS package involves:

1. Creating an initial design

2. Analyzing the present design

3. Evaluating the objective function for the present design

4. Modifying the present design

5. Return to step 2 until an optimum design is determined

Implementing an optimization problem involves defining the design variables, the state variables, and the objective function for the optimization. The design variables are the variables that will be altered by the optimization routines in order to find the combination of these variables that will optimize the specified objective function. The state variables are parameters that are dependent on the design variables. For this analysis, the design variables include:

1.   Magnet Height

2.   Winding Slot Span

3.   Back Iron Thickness

4. Magnet Span

The state variables include

1. Magnet Thickness

2. Magnet Gap

3. Stator Tooth Width

4. Stator Slot Width

The area of the slot is determined by the number of turns necessary and the wire size selected. For this design, wire size AWG 22 was selected. The selection was based on a tradeoff between the area necessary for the required number of turns and the resistance of the winding. AWG 22 was determined to be the best choice given these criteria. Thus, the slot height was determined by the fixed area and the state variable for the slot width.

The objective function for this analysis is established to maximize the air gap flux in the machine. By maximizing the air gap flux, the output voltage of the machine and the output power of the machine can be maximized for the given machine diameter as established above.

Performing the ANSYS analysis and optimization of the parametrically defined model of the linear alternator resulted in the following parameters

Table 2-2. Optimized Alternator Parameters

Magnet Thickness	1.485	Inches
Magnet Gap	0.165	Inches
Tooth Width	0.825	Inches
Slot Width	0.825	Inches
Back Iron Thickness	0.579	Inches
Air Gap	0.065	Inches
Magnet Inner Diameter	1.65	Inches
Magnet Outer Diameter	2.92	Inches

Magnet suppliers were contacted to provide prices for magnets of the dimensions determined by the ANSYS optimization. Having magnets made to fit the exact dimensions proved to be overly expensive for a prototype alternator design. However, discussions with the various magnets suppliers indicated that magnets could be provided at substantially lower price if the dimensions were selected to correspond with magnetic material in stock with the suppliers. So, the design process was reversed in such a way that the magnet dimensions became the independent variable in the system, and the machine output power was calculated based on the available magnets. The stock magnets that came closest to matching the desired specifications had an outer diameter of 2.475 inches and an inner diameter of 1.025 inches. The thickness of these magnets was made to the specifications, as they were constructed from several rings. Using these sizes for the magnets and recalculating the design results in the following design parameters.

Table 2-3. Alternator Parameters

Output Power	S_n	488	W
Output Voltage	V_0	120	V_{RMS}
Number of Active Rotor Poles	m_r	4	Poles
Pole Pitch	τ	1.65	Inches
Specific Thrust	f_{xr}	1.32	N/cm^2
Machine Speed	U	1.4	m/s
Predicted Rated Efficiency	η	0.80	
Magnet Air Gap Flux Density	B_{gr}	0.65	T
Diameter	D	2.475	Inches
Number of Windings	N_s	296	Turns

Dynamic Simulation using Finite Element Analysis

Once the model was optimized using the ANSYS package, the dynamic performance was examined using a combination of the Maxwell package and software developed in house. The parametric capabilities of the Maxwell package proved to be

much easier to implement than those in the ANSYS for the dynamic simulation. Thus, the decision was made to utilize the Maxwell package for this simulation.

To begin the dynamic simulation of the PM linear alternator, the optimized model found using ANSYS was put into the Maxwell software. Constraints were then placed on the model to allow the translator of the machine to be moved relative to the machine stator by the parametric processor in the Maxwell software. Maxwell was used to position the stator at an arbitrary base position which was defined as y=0. At this point, the model was analyzed to determine the flux linkages for each coil as well as the force exerted on the translator. The parametric component then moved the translator an incremental distance and analyzed the model again. This process was repeated until the translator had moved one full pole pitch through the stator.

This simulation procedure provided the value of the flux linkages for each coil and the force exerted on the translator as the translator position varied. In the original design, the teeth of the stator were to be laminated steel teeth. The initial analysis on this design indicated that the reluctance force in the machine was much too high for the prototype engine. Therefore, the decision was made to convert from an iron core machine to an air core machine. The following results are for the air core machine. The flux linkage data was then put into a spreadsheet so the machine output voltage could be calculated. Faraday's law, which stated that the magnitude of the voltage induced on a coil is equal to the time rate of chance of the flux linking the coil and is shown in Equation 2-4, governs the determination machine output voltage.

$$V = \frac{d\lambda}{dt} = N\frac{d\phi}{dt} \qquad (2\text{-}4)$$

where

λ = total flux linking coil

ϕ = flux linking a single coil

N = Number of turns in the coil

So, the voltage induced on each coil in the alternator can be found using Equation 2-4, if the number of coils, and the time derivative of the flux is known. In this case, the number of coils is known, but the time derivative of the flux, $\frac{d\phi}{dt}$, is not directly known.

Rather, a discrete estimate of the position derivative of the flux, $\frac{d\phi}{dt}$, is known from the flux linkage data from Maxwell. Additionally, the time derivative of the translator position, $\frac{dx}{dt}$, is known by establishing the velocity profile of the translator. The velocity profile of the translator was assumed to be some linear combination of a constant speed with instantaneous reversal and a sinusoidal speed. The program allowed for altering the relative contributions of each of these portions to the total speed profile. For the tests conducted, the speed profile used was a true sinusoidal velocity profile.

With the position derivative of the flux, $\frac{d\phi}{dt}$, and the time derivative of the translator position, $\frac{dx}{dt}$, the time derivative of the flux can be found as shown in Equation 2-5.

$$\frac{d\phi}{dt} = \frac{d\phi}{dx}\frac{dx}{dt} \quad (2\text{-}5)$$

Defining the time derivative of the translator speed as the velocity of the machine, Equation 2-5 can be rewritten as

$$\frac{d\phi}{dt} = \frac{d\phi}{dx}v \quad (2\text{-}6)$$

Then, the machine output voltage, V, can be found by substituting Equation 2-6 into Equation 2-4 to get

$$V = N\frac{d\phi}{dx}v \quad (2\text{-}7)$$

Equation 2-7 was then used to determine the output voltage induced on each of the five coils in the alternator.

Alternator Mechanical Construction and Design

Once the parameters were found that resulted in the desired alternator performance were determined, the mechanical structure of the machine could be designed based on these dimensions. The tubular structure of the linear alternator body was designed using steel mechanical tubing. The tubing functions as both the back iron of the machine as well as serving as a structural support member for the windings and teeth of the alternator. The thickness of the back iron was increased from the specified thickness to 0.5 inches to allow for simpler construction. The increase was necessary to gain the additional thickness necessary to allow the ends of the tube to be tapped so the endplates could be bolted directly to the back iron tube. Increasing the thickness of the back iron will not have a significant effect on the operation of the alternator. In fact, the extra thickness can only improve the electrical operation as the reluctance is reduced by the greater cross sectional area of the back iron.

To construct the back iron tube, a section of mechanical tubing that had a larger outer diameter and a smaller inner diameter than necessary was selected. This tube was then cut in half lengthwise to form two half shells. The two half shells were created to

make the final construction of the alternator simpler. The two half shells were then clamped together and turned to the desired inner and outer dimensions in a lathe. A slot was then machined in one side of the back iron tube to allow for electrical connection to the windings of the machine. Removal of part of the back iron will have a slight effect on the reluctance, and therefore the performance of the machine, but the extra thickness of the back iron over the specification should compensate for the slot. Moreover, the advantage of being able to test various coil and winding configurations without having to rework the back iron tube far outweighs the slight performance degradation which might result from removal of the material in the slot. Endplates were then machined to bolt directly to the ends of the back iron tube. The opening in the endplates was made smaller than the inner diameter of the tube so the endplates would hold the windings and teeth securely inside the tube. The coils for the machine were wound to have the desired number of turns and fit in the specified dimensions. The inner diameter of the coils matched the outer diameter of the magnets plus the dimension of the air gap. The outer diameter of the windings matched the inner diameter of the back iron tube so the windings fit tightly inside the tube. The steps for construction of the alternator started with putting the windings and the teeth into the bottom half shell of the back iron tube. Since this prototype is to be an air core machine, as previously discussed, the stator teeth were fabricated using Teflon, a non-conductive, non-magnetic material. With the teeth and the windings properly positioned in the bottom half shell, the top half shell was put in place. Then, the endplates were bolted to the back iron tube both to hold the two half shells together and to hold the windings and teeth in place.

The translator construction involved fabrication of an aluminum shaft and sliding the magnets and the aluminum spacers on the shaft. Since opposing poles of the magnets needed to be facing each other, a significant amount of force was necessary to squeeze the translator assembly together. This was accomplished by threading the end of the shaft and using a larger washer and a nut to first put the magnets and spacers in the proper positions and then to hold the in place. The translator assembly was then carefully inserted into the alternator assembly.

Conclusions

An idealized model of a linear engine, consisting of two pistons linked by a solid rod, was used to investigate the relationship between stroke, compression ratio, and operating parameters. A benchtop model was constructed and used to provide two-stroke, port-injected, spark-ignited operating data. Pressure-volume diagrams for no load conditions, and loaded conditions, with advanced timing, showed adverse work where pressure in the latter part of the outward stroke exceeded that at the beginning of the inward stroke. This adverse work can be eliminated with operation at high loads and retarded timing. The engine can produce approximately 780 W of positive power in sustained operation. The experimental linear engine was integrated with a permanent magnet alternator, and successful operation was sustained at an electrical output of 316 W at 23.1 Hz (1386 cycles/minute). The maximum measured power produced by the engine-alternator combination was found to be less than the power produced by the engine alone under friction braking. This is explained by the electrical alternator efficiency, as well as differences in engine operation between the two tests.

A copy of Cawthorne's masters thesis is attached with further analysis and results. The development of a diesel-fueled two-stroke linear engine is discussed in the next section.

Compression Ignited Linear Engine Development

Introduction

The prior research discussed above has shown that the operation of a linear free piston engine with a throttle, while possible, is undesirable (Nandkumar, 1998; Cawthorne, 1999). A diesel linear engine prototype has been developed for electrical power generation. The two-stroke engine prototype, with a bore of 75mm and a maximum stroke of 71mm has been designed and constructed but has not achieved sustained operation at time of writing this report (Houdyschell, 2000).

Diesel Engine Modeling and Analysis

Considering that the spark-ignited engine was a proof of concept design, and was used to validate preliminary models, the modeling undertaken for the compression-ignition engine was much more involved (Petreanu, 2001).

Dynamic Modeling

Consider the case of a linear engine with two reciprocating pistons linked by a solid shaft that oscillate back and forth in a left-to-right motion. The reciprocating mass represented by the pistons, piston rings, connecting rod, and the magnets, can be reduced to a mechanical system schematically represented in the figure from below. Equation 3-1 describes the motion of the system.

$$m \frac{d^2x}{dt^2} = \sum_i F_{i_r} \qquad\qquad (3\text{-}1)$$

The right hand side of equation 3-1 represents the summation of the forces that act in the plane of motion. The only forces are considered to act on the moving assembly are the resultant pressure forces given by the difference between the pressures in the two

cylinders, a frictional force, and the load. The load represents the electromagnetic force introduced by the linear alternator coupled to the linear engine.

Thus, the above equation can be written as

$$m\frac{d^2x}{dt^2} = F_p - F_f - F_l \qquad (3\text{-}2)$$

where F_p represents the resultant pressure force,

F_f is the friction force, and

F_l is the electromagnetic force.

The integration of this differential equation will permit us to determine the equation of motion for the linear engine. The analytic integration is very difficult due to the complex variation of the three forces in space and time. The piston assembly does not follow a prescribed motion but rather its resultant motion is established as a result of the net balance in the applied forces. Thus, the numerical integration is imposed.

Although the linear engine is crankless, the frictional force cannot be neglected. The friction in this case is attributed to the piston assembly only. There have been several studies with regards to the friction in the internal combustion engine, and according to these, the piston assembly friction represents the major source of engine mechanical friction. Elements of the piston assembly that contribute to friction are the piston rings and the piston skirt. There is also friction in the wrist pin that should be noted even though it is small in comparison to the other friction forces previously mentioned. In linear engines, wrist pin and skirt forces will be negligible. Descriptions of the causes of friction for internal combustion engines and design solutions towards diminishing the effects of the frictional phenomena were researched. Experimental work has shown that

the friction coefficient varies between 0.2 for boundary lubricated engine components to 0.001 for hydrodynamically lubricated engine components. According to lubrication theory there are three lubrications regimes, and these are known as boundary, hydrodynamic, and mixed lubrication. In the boundary lubrication regime the friction is proportional to the normal load applied and this is referred as the Coulomb friction.

$$F_f = c_f \cdot N \qquad (3\text{-}3)$$

where c_f is the coefficient of friction, and

N is the normal load

Although the lubricant is present between the two surfaces, the coefficient of friction is independent of the bulk lubricant viscosity, the sliding speed and the unit load. The hydrodynamic regime occurs when the two surfaces in relative motion in the presence of a lubricant between the two surfaces, have no physical contact. The resistance to motion results from the shear forces within the film.

The shear stress τ, developed in a liquid film between two surfaces in relative motion is given by

$$\tau = \mu \frac{dU}{dy} \qquad (3\text{-}4)$$

where μ is the fluid dynamic viscosity, and $\frac{dU}{dy}$ is the velocity gradient across the film.

The friction in the hydrodynamic regime depends on geometry, speed and lubricant viscosity, and the fiction force has the form

$$F_f = \frac{\mu A U}{\delta} \qquad (3\text{-}5)$$

where μ is the fluid viscosity,

A is the area,

U is the relative velocity, and

δ is the film thickness.

The mixed lubrication regime occurs when the film thickness becomes thinner than the asperities of the two surfaces. This way the two surfaces in relative motion have a physical contact, therefore to the viscous friction is added the solid friction effect. The physical contact of the two surfaces is realized through the peaks of the asperities. This lubrication regime is illustrated in figure 3-1.
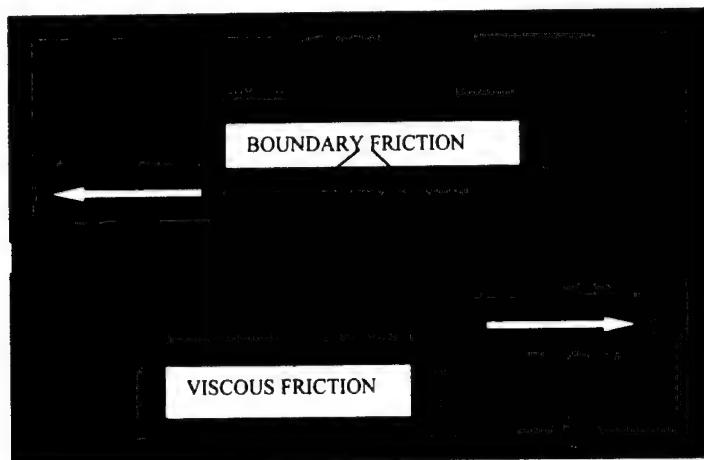

Figure 3-1. Illustration of different lubrication regimes.

As it was mentioned before, the piston assembly represents the only friction source for case of the Linear Engine. Elements of the piston assembly, which contribute to the friction, are the piston rings, the piston skirt and the wrist pin. The analyses developed on the piston assembly friction showed that the ring friction has a dominant aspect. Heywood presents a friction analysis for the case of a piston ring in hydrodynamic regime. Based on the assumption that the piston ring operates in hydrodynamic regime, the frictional effects can be evaluated from the Reynolds equation:

$$\frac{\partial}{\partial x}\left(h^3 \frac{\partial p}{\partial x}\right) = 6U\mu \frac{\partial h}{\partial x} + 12\mu \frac{\partial h}{\partial t} \qquad\qquad (3\text{-}6)$$

where h is the instantaneous film thickness.

This equation, along with the appropriate force balance on the ring, can be solved for the couple film and ring behavior.

The calculation of the friction force for the experimental model is a very complicated process; thus the use of an existing correlation permits a faster evaluation far the friction forces. An empirical expression for the calculation of the friction mean effective pressure was used. This correlation, used for the evaluation of the friction force for the SI model, is a function of engine stroke length and speed.

$$fmep = a + bL_{st}N \qquad\qquad (3\text{-}7)$$

where a and b are constants,

L_{st} is the stroke length in meters

N is the engine speed in cycles/min

The constants a and b have different values based on the type of the engine, size of the engine, and also based on the type of the bearing (with rolling element or plain). For the case of a rolling element the value of the constant a is zero. In the previous work the calculation of the friction force was based on the same correlation.

Thermodynamic Modeling

Mathematical models have been developed to enhance understanding of the flow field, fuel air mixing, and combustion in internal combustion engines. These models can be classified into two groups: thermodynamic models, also called zero-dimensional models, and dimensional models. Thermodynamic models, which account for the

temporal resolution of the flow field, can also be divided into single-zone zero-dimensional models and multi-zone models. Single-zone models can be used in heat release analyses if an experimental pressure diagram is used as input or as a predictive tool if the heat release rate or the fuel mass burning rate is specified. Single-zone models consider that the mixture composition, temperature, and pressure are uniform throughout the combustion chamber. These models take in account heat transfer losses to the cylinder walls and combustion heat release as functions of time. Single-zone models do not distinguish between burnt and unburned gases. The gas exchange process in single-zone models is handled using quasi-steady one-dimensional equations. Multi-zone models offer a more accurate approach of the thermodynamic properties of the cylinder charge. Multi-zone models account for the temporal and spatial distribution of temperature and concentration (the case of stratified charge). Multi-zone models can be referred as quasi-dimensional since they account for geometric features of the combustion chamber and the flame propagation process, the burned and unburned gases are considered as separate thermodynamic systems that are uniform in composition and state.

Multidimensional models are able to provide temporal and spatial resolution of the flow field. In this type of model, the governing equations (partial differential equations), conservation of mass, conservation of momentum, conservation of energy, and conservation of chemical species, are solved numerically subject to appropriate boundary conditions. Turbulence models are used to account for the inability of the coarse computational grid to resolve small details of the flow field.

Considering the modeled engine as being an open thermodynamic system as shown in figure 3-2.
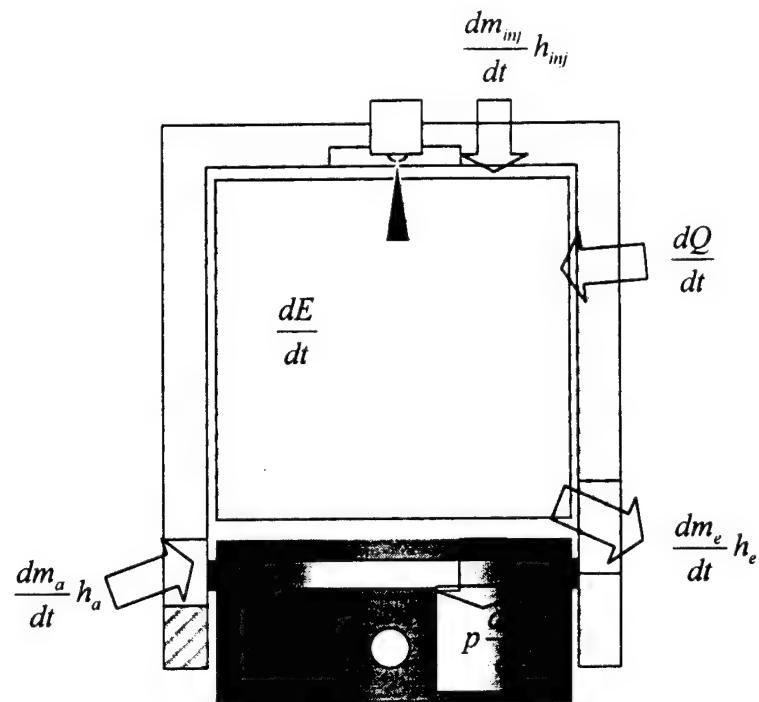
Figure 3-2. First law of thermodynamics applied to the cylinder.

Conservation of Mass

$$\frac{dm}{dt} = \frac{dm_a}{dt} + \frac{dm_{inj}}{dt} + \frac{dm_e}{dt} \tag{3-7}$$

Where $\dfrac{dm}{dt}$ represents the time rate of change of the mass of the system. The right hand side of the equation takes into account the instantaneous mass flow rates in and out of the cylinder, the mass flows into the system being considered positive.

Conservation of Energy

$$\frac{dE}{dt} = \frac{dQ}{dt} - p\frac{dV}{dt} + \sum_i \dot{H}_i - \sum_e \dot{H}_e \qquad (3\text{-}8)$$

$$\sum_i \dot{H}_i = \frac{dm_a}{dt} h_a + \frac{dm_{inj}}{dt} h_{inj}$$

$$\sum_e \dot{H}_e = \frac{dm_e}{dt} h_e$$

where $\frac{dU}{dt}$ represents the time rate of change of the internal energy of system (cylinder

gases),

$\frac{dQ}{dt}$ is the rate of heat transfer to the system,

$p\frac{dV}{dt}$ is the rate of work done by the system, and

$\sum_i \dot{H}_i$ and $\sum_e \dot{H}_e$ is the enthalpy flux into and out of the system respectively.

Scavenging Process Modeling

The Linear Engine works based on the two-stroke cycle and the mechanical

arrangement of the cylinders is similar with a two-stroke engines, thus the gas exchange

process can be approach in the same manner as for a two-stroke engine. The

distinguished characteristic of operation of the two-stroke engine is that each outward

stroke of the piston is a working or expansion stroke. To achieve this operating cycle, the

fresh charge must be supplied to the engine cylinder at a pressure high enough to displace

the burnt gases from the previous cycle. This pressure can be achieved by using an

additional device, usually a scavenging pump or a compressor. The operation of clearing

the cylinder of burnt gases and filling it with fresh mixture for SI engines, and air for CI

engines, is called scavenging. The scavenging process can be considered as a multiphase process, the first phase being the blowdown process, and the second phase the scavenging process itself. Two-stroke engines are classified on the basis of what the air path or flow arrangement is during the course of scavenging.

There are three groups of scavenging flow arrangements, cross-scavenged flow, loop-scavenged flow, and uniflow-scavenged. The first two categories of flow arrangement use inlet and exhaust ports in the cylinder wall, which are uncovered as the piston moves outwards. In the last case the cylinder has inlet ports and exhaust valve(s).

Due to the mechanical arrangement of the Linear Engine cylinders, the flow arrangement proposed for this study will be a loop-scavenged flow. The solution for a loop-scavenged flow has been chosen due to it simplicity, a uniflow-scavenging process would complicate the mechanical arrangement of the cylinder since it involves the presence of an exhaust valve.

To measure the success of the scavenging process, or to evaluate the performance of this process, the following parameters are used:

The delivery ratio Λ

$$\Lambda = \frac{\text{Mass of delivered charge}}{\text{Displaced volume} \times \text{Ambient density}}$$

The charging efficiency η_c

$$\eta_c = \frac{\text{Mass of delivered charge retained}}{\text{Displaced volume} \times \text{Ambient density}}$$

The scavenging efficiency η_s

$$\eta_s = \frac{\text{Mass of delivere charge retained}}{\text{Mass of trapped cylinder charge}}$$

The trapping efficiency Γ

$$\Gamma = \frac{\text{Mass of delivered charge retained}}{\text{Mass of delivered charge}}$$

The relative charge R_c

$$R_c = \frac{\text{Mass of trapped cylinder charge}}{\text{Displaced volume} \times \text{Ambient density}}$$

The scavenging efficiency can be expressed as the product between delivery ratio Λ, and the trapping efficiency Γ.

$$\eta_s = \Lambda \cdot \Gamma \qquad\qquad\qquad (3\text{-}8)$$

Also, the charging efficiency η_c can be expressed as the product between the relative charge R_c, and the scavenging efficiency η_s.

$$\eta_c = R_c \cdot \eta_s \qquad\qquad\qquad (3\text{-}9)$$

The modeling of the scavenging process represents a complex task since the scavenging process itself is a complex process. The scavenging process deals with unavoidable phenomena such as mixing and short-circuiting, these two processes diminish the success of the scavenging process (Heywood, 1988).

Mathematical models for the scavenging process can be classified in three categories: one-phase models, multi-zone models, and multidimensional models. For the case of one-phase models, there are two limiting ideal models for the scavenging process. The first is the perfect displacement model, and the second one is the perfect mixing model. The perfect displacement model assumes that the process occurs at constant cylinder volume and pressure, the burned gas is perfectly displaced by the incoming fresh charge, no mass or heat is allowed to cross the interface between the fresh

charge and the burned gas. Another assumption of this model is that the cylinder walls are adiabatic.

Based on these assumptions, the model yields the following the expression for the charging efficiency and for the scavenging efficiency:

$$\eta_c = \begin{cases} \Lambda & \text{for } \Lambda < \dfrac{\rho_a}{\rho_0} \\[4mm] \dfrac{\rho_a}{\rho_0} & \text{for } \Lambda \geq \dfrac{\rho_a}{\rho_0} \end{cases} \qquad (3\text{-}10)$$

$$\eta_s = \begin{cases} \left[1 + \dfrac{\rho_b}{\rho_a}\left(\dfrac{1}{\lambda}\dfrac{\rho_a}{\rho_0} - 1 \right) \right]^{-1} & \text{for } \Lambda < \dfrac{\rho_a}{\rho_0} \\[4mm] 1 & \text{for } \Lambda \geq \dfrac{\rho_a}{\rho_0} \end{cases} \qquad (3\text{-}11)$$

where ρ_a is the fresh charge density,

ρ_b is the burned gas density,

ρ_0 is the ambient density, and

Λ is the delivery ratio,

The perfect mixing model assumes that the scavenging process is a perfect mixing process, the incoming fresh charge instantaneously mixes with the cylinder burned gas to form a homogeneous mixture of perfect gases. Heat transfer is not allowed between the cylinder mixture and the cylinder walls, and as in the case of the perfect displacement model the process occurs at constant cylinder pressure and volume. The gas that exits the cylinder exhaust port is a mixture of fresh charge and burned gas. The above assumptions lead to the following relations for the charging efficiency and for the scavenging efficiency:

$$\eta_c = 1 - \exp(-\Lambda) \tag{3-12}$$

$$\eta_s = \frac{T}{Ti}[1 - \exp(-\Lambda)] \tag{3-13}$$

The before presented one-phase models represent a very fast and simple toll in the modeling work, but they are not realistic, the real scavenging process being more complicated. In fact the real scavenging process represents a combination of the two described ideal models. According to recent research, the scavenging process may be approximated to proceed in three phases; displacement mixing and short-circuiting. The short-circuiting occurs when the fresh charge exits the exhaust port without interaction with the cylinder burned gas. Multi-zone models account for this phases scavenging process. Multi-zone models consider the cylinder divided in two, three or more zone such as fresh charge zone, burned gas zone, and mixed fresh charge and burned gas zone. The multi-zone models generally use the following assumptions:

The in-cylinder pressure is uniform.

Each zone has a uniform temperature, but it can be different for each zone.

There is no heat transfer from one zone to another.

Other models proposed are multi-zone models in which the cylinder was divided in two zones, a mixing zone adjacent to the intake port, and a burnt gas zone adjacent to the exhaust port. In this model it is also assumed that the process occurs at constant cylinder volume, pressure, and temperature. Another assumption was that at the interface between the two zones there is no heat or mass transfer. The short-circuiting phenomena was also taken into consideration, considering that the short-circuited fresh-charge represents a portion of the scavenged air.

A scavenging model has been developed considering the cylinder charge divided in three zones: a fresh charge zone, a burnt gas zone, and a mixing zone. In this model it is considered that the scavenging process takes place in three phases: a displacement phase, a short-circuiting phase, and a mixing phase. In the first phase the fresh charge enters the cylinder and displaces the cylinder content. The exhaust gas does not contain any fresh charge, and the mixing process occurs at the only at the boundaries of the incoming charge. In the second phase the mixing process continues and the incoming charge is short-circuited and it represents the only component that passes the exhaust ports. In the third phase a homogeneous mixture of fresh charge burned gas leaves the cylinder.

The hydrodynamic or multidimensional models offer the best description of the scavenging process. The hydrodynamic models account for the time variation of the spatial profiles of the temperature, mixture composition, and flow field. These can be obtained by solving a set of differential equations e.g. conservation of mass, conservation of momentum in one, two or three coordinates, conservation of energy.

Combustion Process Modeling

From the previous experiment and data analysis, in the case of the spark-ignited linear engine, it was shown that the combustion process for Linear Engine is critical, therefore the combustion process modeling requires full understanding of real process from the one involved in this work.

The combustion cylinder of the proposed linear engine is a direct injection compression ignition engine, and therefore the models presented in this section will refer only to compression ignited engines.

Heywood (1988) presents the features of the combustion process in compression ignition engines as follows. The liquid fuel is injected at high pressure and velocity into the engine cylinder. The injected fuel atomizes in small droplets and penetrates the air mass from the combustion chamber. The fuel vaporizes and mixes with the high-temperature and high-pressure air in the cylinder, creating flammable volumes. Since the air temperature and pressure are above the ignition point of the fuel, spontaneous ignition of the portions already mixed occurs after a delay period from the start of injection. As the combustion of these regions occurs, the cylinder temperature and pressure rises. The consequent compression of the of the unburned portion of the charge shortens the delay period before ignition for the fuel and air which has mixed to within combustible limits, which then burns rapidly. Injection continues until the desired amount of fuel has entered the cylinder. The atomization, vaporization, fuel-air mixing, and combustion continue until all the fuel has passed through each process. In addition, mixing of the air remaining in the cylinder with burning and already burned gases continues throughout the combustion and expansion processes. The combustion process in compression ignited engines depends on the combustion chamber geometry, the fuel injection system, and on the engine's operating conditions. From this summary it can be understood that the combustion process in compression ignition engines represents a very complex process. The combustion process in compression ignition engines, can be considered as having three distinct main stages and those are, the ignition delay, the premixed combustion, and the diffusive combustion

Ignition Delay

The ignition delay represents the period of time from the beginning of fuel injection and the start of combustion. The ignition delay can be considered as having a physical component and a chemical component. The physical component accounts for the atomization of the liquid fuel jet, the vaporization of the fuel droplets, and the mixing of fuel vapor with air. The chemical component of the ignition delay accounts for the mechanism of chemical processes involved in the autoignition. The chemical processes depend on the fuel characteristics and composition, the cylinder charge pressure and temperature, as well as on the physical processes enumerated above which govern the distribution of fuel throughout the air charge. Although the ignition delay has been the subject of many studies, it cannot be predicted accurately. In different models, there are different expressions for the ignition delay, most of them based on empiric relations, and most models have a certain mathematical correlation for the ignition delay expression. The following expression has good results for direct injection engines and is a function of cylinder pressure, temperature, mean speed, and also a function of fuel characteristics.

$$\tau_{id} = \frac{0.36 + 0.22\bar{S}_p}{0.006N} \exp\left[E_a\left(\frac{1}{RT} - \frac{1}{17{,}190}\right)\left(\frac{21.2}{p - 12.4}\right)^{0.63}\right] \tag{3-14}$$

where τ_{id} is the ignition delay in $\sec \times 10^{-3}$

$\bar{S}_p$ is the mean piston speed in m/s,

N is the engine speed in rev/min,

E_a is the apparent activation energy in J/mole,

T is the cylinder charge temperature in degrees Kelvin, and

p is the cylinder pressure in 10^5 Pa .

The apparent activation energy is given by

$$E_a = \frac{618,840}{CN + 25}$$

where CN represents the fuel cetane number

Premixed Combustion

The combustion process in this stage is characterized by a high rate of heat release. During the ignition delay period the fuel injection continues and part of the previous injected fuel has mixed with air and has formed some regions of combustible mixture. The region that has reached the combustion requirements burn quickly, and therefore the cylinder pressure and temperature increase aiding the continued vaporization of the remaining liquid fuel. As mentioned before, this stage is associated with high heat release rates.

Diffusive Combustion

The diffusive combustion represents the phase of the combustion process in which the process itself is controlled by the rate at which the mixture becomes available. The fuel vapor-air mixing process controls this phase of the combustion process. Compared to the premixed combustion, in which the fuel encounters a rapid oxidation and thus a rapid pressure rise, the diffusive combustion stage has a steady aspect with regards to the pressure variation and the heat release rate.

Single-zone Models

Single-zone models yield a system of ordinary differential equations for the mixture pressure, temperature and mass. These models do not account for the presence of vaporizing liquid droplets, fluid flow, combustion chamber geometry, and spatial variations of the mixture composition and temperature. In single-zone models the

cylinder charge is assumed to be a homogeneous mixture of ideal gases. Considering the cylinder an open system, the state of the mixture can be described at every instant by the pressure p, temperature T, and equivalence ratio ϕ.

The mass fraction burned is most commonly expressed by using the Wiebe Function.

$$\chi(t) = \frac{m_b}{m_{inj}} = 1 - \exp\left[-a\left(\frac{t-t_0}{Cd}\right)^{b+1}\right] \qquad (15)$$

where χ is the mass fraction burned,

m_b is the mass burned,

m_{inj} is the mass injected,

a and b are shape factors,

t_0 is the time at which the combustion process starts, and

Cd is the combustion duration.

Multi-zone models

In comparison to the single-zone models where the cylinder mixture is considered homogeneous, in the multi-zone models the cylinder mixture is divided into burning and nonburning zones, each zone being treated as separate thermodynamic system. These models account for air entrainment and fuel jet penetration. In the multi-zone models the burnt zone corresponds to the injected fuel, and the unburnt zone corresponds to the surrounding air. The fuel jet penetration and the air entraining process are in most cases based on empirical relations. Two-zone models attribute the burnt zone to the injected fuel assuming that the injected fuel represents a uniform gaseous medium. Processes such as atomisation and evaporation of the fuel droplets are completely neglected, therefore the accuracy of two-zone models is limited. More complex multi-zone models,

which consider more than two zones, account for the fuel jet characteristics by dividing the fuel spray injected into the cylinder into parcels which are analysed separately. Although multi-zone combustion models vary in complexity, the main strategy is to model the fuel jet into various elements (zones) which entrain air and ignite as the mixture is prepared for combustion. In this type of model, simplified quasi-steady equations are used to describe various processes of fuel injection, atomisation, droplet formation, air entrainment, droplet evaporation, ignition, heat release, and heat transfer. Despite that they present a certain degree of empiricism, multi-zone models are powerful tools in predicting with accuracy the exhaust emissions.

Multidimensional Models

More complex than the zero-dimensional models, the multidimensional models of diesel engine combustion account for engine geometry and the spatial and temporal variation of the flow field, temperature, composition, pressure, and turbulence within the combustion chamber. The multidimensional models are based on computational fluid dynamics (CFD) computations. In these models the governing equations that describe the flow field are solved numerically with different numerical schemes. The KIVA code, for example, has the ability to calculate three-dimensional flows in engine cylinders with arbitrary shaped piston geometries, including the effects of turbulence, sprays and wall heat transfer. These particular models based on are very expensive since they require high computational resources.

Chemical Kinetics Based Models

The last category of models used in combustion modelling are represented by models that are based on the chemical equations governing the combustion process. In

these models, the combustion process is considered the result of a series of chemical reactions, called reaction mechanisms, through which the cylinder charge is transformed into products of combustion. In the chemical process of combustion the fuel is broken down and the constituent atoms combine in different ratios and at certain rates. However, since there are millions of atoms that undergo billions of combinations, it is practically impossible to predict with accuracy what occurs. Chemical kinetics models can be classified based on the type of kinetic mechanism employed as detailed or reduced. The detailed chemical kinetics models include a large number of possible chemical reactions that characterize the combustion process. Complete detailed reaction schemes are only available for the simpler hydrocarbon fuels such as methane, propane or butane, for the blended hydrocarbon fuels the detailed chemical mechanisms are not completely known. However, these models are very complex due to the large number of chemical reactions involved, and also expensive, since they require a large amount of computational resources. More often used due to their relative simplicity are the reduced or simplified chemical kinetics models, in these models the combustion process is considered to be governed by a series of chemical reactions, which consists of a reduced number of chemical reactions. Reduced schemes of varying degrees of details require much less computational resources.

A chemical equation for the combustion of a fuel has the following form

$$C_aH_b + \alpha(O_2 + 3.773N_2) \rightarrow \beta CO_2 + \delta H_2O + \varepsilon N_2 + \gamma CO + $$
$$+ \eta NO + \kappa OH + \mu H + \nu C_xH_y + ... \tag{3-16}$$
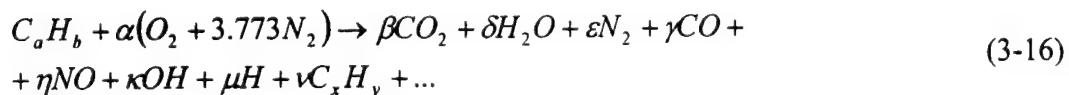
The fuel oxidation represents a complex process, it occurs in many steps called base reactions. The simplest base reaction can be written as follows

$$\alpha A + \beta B \leftrightarrow \delta C + \gamma D \tag{3-17}$$

where A, B ,C, and D represent the chemical species of the reaction, and

α, β, δ, and γ are the corresponding stoichiometric coefficients.

According to the law of mass action, the rate at which product species are produced and the rate at which reactant species are removed is proportional to the product of the concentrations of reactant species, with the concentration of each species raised to the power of its stoichiometric coefficient.

$$R^+ = -\frac{d[A]^+}{dt} = \frac{d[C]^+}{dt} = k^+[A]^\alpha[B]^\beta \tag{3-18}$$

$$R^- = -\frac{d[C]^-}{dt} = \frac{d[A]^-}{dt} = k^-[C]^\delta[D]^\gamma \tag{3-19}$$

where R^+ and R^- represent the forward and backward rate respectively, and

k^- and k^+ represent the proportionality constants for forward and backward rate respectively.

More generally, any reaction can be written as

$$\sum_{i=1}^{n} v_i M_{R_i} \leftrightarrow \sum_{i=1}^{m} v_i M_{P_i} \tag{3-20}$$

where v_{R_i} and v_{P_i} represent the stoichiometric coefficients of the species M_i, and

subscripts R and P denote reactants and products respectively.

The rate of reaction for a chemical reaction when the process undergoes forward can be written as

$$R^+ = -k^+\prod_{i=1}^{n}[M_{R_i}]^{v_{R_i}} \tag{3-21.a}$$

Similarly the backward rate for a chemical reaction can be expressed as

$$R^- = -k^- \prod_{i=1}^{m} [M_{P_i}]^{v_{P_i}}$$ (3-21.b)

The brackets indicate the appropriate concentration quantity such as molarity or partial pressure. The proportionality constant also called the specific reaction-rate constant is independent of the concentration and it depends only on the temperature. The specific reaction-rate constant is given by Arrhenius law:

$$k = A \exp\left(-\frac{E_a}{RT}\right)$$ (3-22)

where A is Arrhenius constant,

E_a is the activation energy,

R is the universal gas constant, and

T is the absolute temperature

The Arrhenius constant also called the collision frequency factor accounts for the effect of collision terms, $A = BT^{\alpha}$. The exponential term is the Boltzmann factor, specifying the fraction of collisions that have an energy greater than the activation energy E_a.

The net rate if removal of reactant species M_{R_i} is

$$-\frac{d[M_{R_i}]}{dt} = v_{R_i}\left(R^+ - R^-\right)$$ (3-23.a)

and the net rate of production of product species M_{P_i} is

$$\frac{d[M_{P_i}]}{dt} = v_{P_i}\left(R^+ - R^-\right)$$ (3-23.b)

When chemical equilibrium is reached, the forward and the backward reaction rates are equal, it then follows

$$K_c = \frac{k^+}{k^-} = \frac{[C]^\delta [D]^\gamma}{[A]^\alpha [B]^\beta} \qquad\qquad (3\text{-}24)$$

where K_c is the equilibrium constant.

In order to evaluate the rate of combustion it is necessary to determine the rate of each individual reaction that characterises a particular chemical kinetic mechanism.

Compression and Expansion Modeling

The compression process for this model is considered to start when the exhaust port closes, and it continues until the start of the fuel injection when, according to the previous discussion, we have considered the start of the combustion process coincides with the start of fuel injection. During this process the cylinder charge receives external mechanical work, increasing its internal energy.

The compression process can be mathematically modeled by using the first law of thermodynamics.

If we neglect the crevice flow, and after some mathematical manipulations the equation becomes:

$$\frac{dQ}{dt} = \frac{\gamma}{\gamma - 1} p \frac{dV}{dt} + \frac{1}{\gamma - 1} V \frac{dp}{dt} \qquad\qquad (3\text{-}25)$$

Neglecting the heat transfer process the equation () reduces to:

$$\gamma p \frac{dV}{dt} + V \frac{dp}{dt} = 0 \qquad\qquad (3\text{-}26)$$

The solution for this differential equation represents the law for an isentropic process.

$$pV^\gamma = Const.$$

The expansion process or the power stroke is considered to start at the end of the combustion process, and ends when the exhaust port opens. The expansion process can be modeled in a similar manner considering the evolution as a isentropic process. In the previous work, the two evolutions were considered as being polytropic processes, and thus they were mathematically expressed as:

$$pV^{m_{c,d}} = Const.$$

$$TV^{m_{c,d}-1} = Const$$

where m denotes the polytropic coefficient, and the subscripts c and d denote the compression and expansion process respectively.

Heat Transfer Modeling

The heat transfer process in an internal combustion engine and particularly for a compression ignition engine represents a very complex process due to the fact that all three forms of heat transfer known are present in the overall heat transfer process, namely conduction, convection, and radiation. For computational simplicity it can be considered that the heat transfer process in the two stroke linear engine is dominated by a convective mechanism.

The modeling of the convective heat transfer process in an internal combustion engine has been a subject to numerous investigations and so far, there are known two types of models, spatially uniform models and, boundary layers models. Spatially uniform models consider the cylinder gases as a uniform medium. More realistic are the boundary layers models, which account for the variation of the physical properties of the in-cylinder gas in a thin layer formed near the cylinder wall. In boundary layer models two regions are considered, one in which the physical properties of the gas are subject to

high gradients, and the other region outside the boundary layer in which the physical properties can be assumed to be uniform. These models are more accurate for the evaluation of the heat transfer process but they require information about the in-cylinder flow-field, fact that can create computational complications. Generally, the equations used for convective heat transfer modeling in internal combustion engine modeling are of the standard convection form

$$\frac{dQ}{dt} = hA\left(T_{cyl} - T_{w}\right)$$
(3-27)

where $\frac{dQ}{dt}$ is the instantaneous heat transfer rate,

h is the heat transfer coefficient,

A is the area over which heat transfer occurs,

T_{cyl} is the cylinder fluid temperature, and

T_{w} is the cylinder wall temperature.

A very accurate evaluation of the heat transfer coefficient represents a very complicate task due to the complexity of the heat transfer process itself, and it does not represent the main priority for this work. Therefore the use of spatially uniform model that uses a heat transfer correlation, a common practice in engine modeling, will be used to simplify the modeling task. There are numerous heat transfer correlations in the IC engines literature, and most of them give satisfactory results despite their empiricism. These correlations relate the Nusselt, Reynolds, and Prandtl numbers in the following general form.

$$Nu = a\,\mathrm{Re}^{d}\,\mathrm{Pr}^{e}$$
(3-28)

where the dimensionless parameters are $Re = \dfrac{\rho v L}{\mu}$; $Pr = \dfrac{\mu c_p}{k}$; $Nu = \dfrac{hL}{k}$; L is the same

characteristic length scale.

Another correlation used, probably the most popular, for the evaluation of the

instantaneous convective heat transfer in IC engines is the one developed by Woschni.

$$Nu = \frac{hL}{k} = 0.035\,Re^m = 0.035\left(\frac{\rho \hat{v} L}{\mu}\right)^m \qquad (3\text{-}29)$$

where Nu is the Nusselt Number,

L is the Characteristic Dimension,

k is the fluid Thermal Conductivity,

Re is the Reynolds Number,

m is the Reynolds Number Exponent.

ρ is the fluid Density,

$\hat{v}$ is the Characteristic Velocity, and

μ is the fluid Viscosity.

In his correlation, Woschni assumed that the ideal gas law was applicable, that the

characteristic dimension was the cylinder diameter D, that m=0.8, that $\mu \propto T^{0.62}$ and that

$k \propto T^{0.75}$.

Substituting these in the Woschni correlation it follows that

$$h = 0.00326 \frac{p^{0.8}\hat{v}^{0.8}}{D^{0.2}T^{0.53}} \qquad (3\text{-}30)$$

where h is the film heat transfer coefficient,

p is the cylinder pressure,

$\hat{v}$ is the characteristic velocity,

D is the cylinder diameter, and

T is the cylinder gas temperature

The characteristic velocity was evaluated throughout different evolutions of the engine cycle as follows.

$$\bar{v} = C_1 \bar{v} + C_2 \frac{V_d T_1}{p_1 V_1}(p - p_{motored}) \tag{3-31}$$

where C_1 and C_2 are coefficients that denote the combustion and motored conditions respectively,

V_d is the displacement volume

$T_1, p_1,$ and V_1 represent the temperature, the pressure, and the volume at ignition,

p is the cylinder pressure, and

$p_{motored}$ is the pressure that corresponds to the motored conditions.

The coefficients C_1 and C_2 have different values based on the process the engine performs.

- Compression $C_1 = 2.28$ $C_2 = 0$

- Combustion and Expansion $C_1 = 2.28$ $C_2 = 0.00324$

- Gas Exchange $C_1 = 6.18$ $C_2 = 0$

The Woschni correlation represents a very fast and convenient tool in the evaluation of the heat transfer, and therefore it will be used for the heat transfer process calculations for a four stroke linear engine model

Diesel Linear Engine Construction and Design

Figure 4-1. shows the structure of a two-stroke compression-ignited linear engine-alternator. The unit is of similar philosophy to the gasoline model previously described.

The cylinders and pistons are from a Kawasaki JS300 engine. The bore is 76mm (2.99inches), with an original intended stroke of 63.5mm (2.5ins). The stroke in the present application is dynamically, rather than mechanically, defined, and could reach a theoretical maximum of around 75mm (3ins), at which point the pistons would contact the heads. The heads are fabricated from aluminum and bolted to the cylinders.
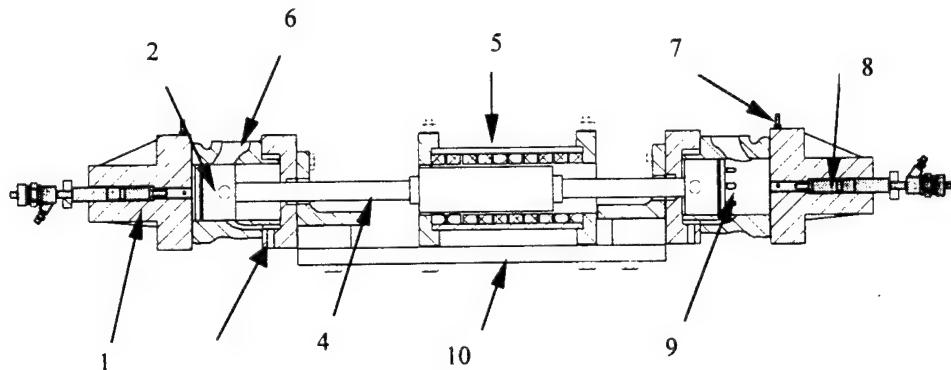

Figure 4-1: Prototype Two-Stroke Diesel Cycle Linear Engine -Alternator

Combination

1. Cylinder Head; 2. Piston; 3. Intake; 4. Connecting Rod; 5. Linear Alternator; 6. Exhaust Port; 7. Glow Plug; 8. Fuel Injector; 9. Intake Ports; 10. Frame;

The connecting rod is aluminum, approximately 760mm (30in) long and 25.4mm (1in) diameter. At each end, it is cross-drilled to accommodate the 18mm (0.7inch) wristpins. The alternator will be mounted to the connecting rod.

Since the linear engine has no rotating components to operate a timed cam, the obvious injection system choice involves a common rail design. Common rail systems are also the most desirable systems for interfacing with electronic control systems and for allowing split injection and injection rate shaping. In the present application, a state-of-the-art Bosch injector, rated to deliver 140mm^3 per stroke at 135MPa (19600psi). In this

application, the injectors are being operated initially at a lower pressure, approximately 69MPa (10000psi), with fuel pressure generated using a hydraulic pump. There is concern that the fuel injected may not autoignite if the cranking compression is not sufficiently high, especially under cold start conditions. To this end, the heads have been equipped with glow plugs, located in the path of the fuel spray, to insure combustion at startup. A photograph of the linear compression–ignited engine model is shown in Figure 4-2.
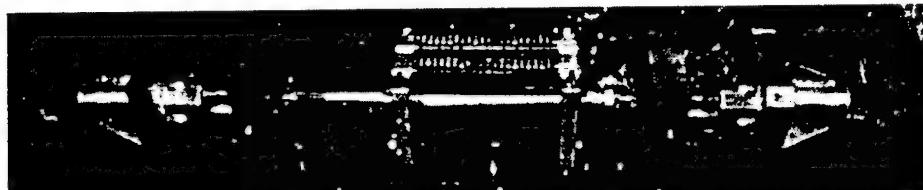

Figure 4-2: Photograph of the Linear Compression–Ignited Engine Model

The heads are also equipped with pressure sensors (PCB Piezotronics type 15A1) to permit realtime modeling of in-cylinder pressure.

Engine Operation

As a first approach, the method adopted to crank the engine was based directly off the gasoline prototype. In that case, the windings of the alternator were configured such that by energizing a certain set of windings, the shaft would move one way, and by energizing a different set, it would move the other way. The transistors used were of the VMOS type, and were rated at 55V 50A. Once the engine was able to sustain regular combustion, it would oscillate close to its resonant frequency. The cranking circuit detected this, and stopped providing current to the windings. These windings were effectively "disconnected" from the transistors by a pair of high current, fast recovery diodes. In the diesel engine, it was realized very early on that this "unipolar" method of connecting the alternator windings wouldn't create sufficient force to generate enough

compression for starting, even assisting the combustion with glowplugs. In this prototype, since the windings were only going to be used to start the engine, and not necessarily for current generation, the windings were reconnected in such a way that each would be used to move the connecting shaft in both directions. The electronics had to be redesigned to power this "bipolar" configuration.

The circuit was built using four identical vertical-process metal oxide semiconductor (VMOS) transistors, rated at 55V 75A, in a bridge configuration. This oscillated the connecting shaft very effectively.

However, the original common-rail diesel injectors that were supplied by the manufacturers couldn't supply the quantity of fuel required for combustion, and the actuating coil of one of these burned out by the very long pulse durations required. A replacement was obtained, but then it was found that the other original injector had also failed. The manufacturers then agreed to supply two additional injectors, but informed us that the shape and size of the replacements would be different. The cylinder heads were re-machined in anticipation of the arrival of the replacements.

After vainly waiting for the injectors from the manufacturers, it was established that Mercedes Benz in Germany was now using injectors similar to the originally supplied ones on their S-class vehicles, and these were now commercially available. Two were immediately ordered, along with two more as spares.

The quantity of fuel injected by these was sufficient to now cause the engine to attempt "sustained oscillation". However, as soon as the shaft reciprocated at speeds higher than the cranking speed, the transistors in the bridge failed spectacularly. This was due to the generated EMF being higher than the design limits of the VMOS transistors.

They were replaced with 100V 75A parts, which now allowed the shaft to sustain oscillation for a few cycles before also blowing out (rather than the one or two that the lower voltage parts could sustain). The bridge was redesigned, incorporating insulated gate bi-junction transistors (IGBTs), rated at 600V 100A. These also met with the same complications incurred with earlier designs. The final design iteration to date incorporates IGBTs rated at 1200V 100A and incorporating new gate protection designs that have allowed for greatly increased cranking durations. A new problem is that with sustained long term cranking, the flexible fuel lines are being called upon to hold greatly increased pressures for extended periods of time, leading to multiple fuel system failures. A solution incorporating hard lines is currently being investigated. Once reliable operation is established, the engine will be operated with variations in load, fuel quantity and injection position. The resulting motion and in-cylinder pressure will be recorded and analyzed.

Conclusion

The linear engine offers the potential to generate and deliver power without the need to convert linear piston motion to rotary crankshaft motion. An idealized model of a linear engine, consisting of two pistons linked by a solid rod has revealed the relationship between stroke, compression ratio, heat input, operational frequency and other parameters. The model shows an increase in the achieved stroke length with an increase in the amount of heat input. The idealized model deals with over-fueling by increasing the stroke of the engine to the maximum. It is believed that this is not how the engine would behave in reality. It is obvious that in the case of over-fueling, incomplete combustion would occur. Also the effects of varying the bore and the sliding mass on operating frequency and power output have been shown for a given heat input. An increase in cylinder bore or slider mass effect the system by increasing the amount of time for a stroke.

The prototype showed successful characteristics in the testing performed. The black smoke attained in some of the later test show that adequate compression was being developed to ignite the fuel with the help of the glow plugs. This is important because it in part proves the feasibility of starting a linear compression ignition engine. The generation of compression upon cranking is the most difficult task to overcome for the compression ignition case.

References

1. Nandkumar, Subhash; "Two-Stroke Linear Engine", Masters Thesis, West Virginia University 1998

2. Cawthorne, William; "Optimization of a Brushless Permanent Magnet Linear Alternator for Use With a Linear Internal Combustion Engine", Masters Thesis, West Virginia University 1999

3. Houdyschell, David; "A Diesel Two-Stroke Linear Engine", Masters Thesis, West Virginia University 2000

4. Petreanu, Sorin; "Conceptual Analysis of a Four-Stroke Linear Engine", Doctoral Dissertation, West Virginia University 2001

5. Heywood, John; Internal Combustion Engine Fundamentals, McGraw-Hill, Inc., 1988